Computational Materials Science 233 (2024) 112712

Contents lists available at ScienceDirect

Computational Materials Science

journal homepage: www.elsevier.com/locate/commatsci

Full length article

An *ab initio* study of vertical heterostructures formed by CdO and SnC monolayers

Mahsa Seyedmohammadzadeh [a], Arash Mobaraki [a], B. Tanatar [a,*], Oğuz Gülseren [a,b]

[a] Department of Physics, Bilkent University, Ankara 06800, Turkey
[b] TÜBİTAK Research Institute for Fundamental Sciences, 41470 Gebze, Turkey

ARTICLE INFO

Keywords:
2D materials
Hetero-bilayers
First-principles calculations
Phonons
Electronic structure
Excitons

ABSTRACT

Assembling two dimensional (2D) materials in vertical heterostructures is one of the main techniques for tuning electronic and optical properties. In most cases, known as van der Waals heterostructures (vdWHs), the interlayer distances are larger than typical covalent bond lengths resulting in weak interlayer interactions. It has been shown that reducing the distance between the layers can significantly alter the properties of separated layers, which is not so noticeable in vdWHs and thus creates a new platform for controlling the physical properties of 2D materials. Motivated by enhanced properties of 2D vertical heterostructures, employing ab-initio calculations based on density functional theory we examined CdO/SnC systems in four different configurations. Our results reveal that in spite of thermodynamic and mechanical stabilities of all considered structures, according to the calculated phonon frequencies, only the structure formed by placing the Sn atom on the O atom and the C atom on the Cd atom is dynamically stable at zero temperature. This structure has an interlayer distance of 2.52 Å which is smaller than the interlayer distance in typical vdWHs. We investigated the electronic and optical properties of this dynamically stable structure utilizing GW approximation and solving Bethe–Salpeter equation. Unlike the monolayer CdO which possesses a single optical absorption peak close to the red light energy, the considered CdO/SnC structure has an optical band gap of 1.14 eV, and it can absorb 13% of incident light in the blue light region.

1. Introduction

Since the exfoliation of single-layer graphene [1] and the demonstration of its distinguishing physical properties from bulk phases of carbon [2,3], a tremendous amount of investigations have been carried out to examine two-dimensional materials (2D) with different functionalities. Currently, a plethora of 2D materials, from insulators to metallic structures, are fabricated or theoretically predicted [4–9].

Alongside the prediction and synthesizing of novel 2D systems, controlling the fundamental band gap and the shape of the band structure of 2D materials is one of the main topics of ongoing researches [10]. The feasibility of band gap engineering by mechanical deformation [11,12], applying external electric field [13] or doping and surface passivation [14] is already demonstrated in several reports [10]. In this regard, assembling 2D monolayers (MLs) in vertical heterostructures is one of the intriguing methods for creating structures with enriched electronic, optical, and magnetic properties [8]. The pioneering examples are the layered structure of graphene, transition metal dichalcogenides (TMDs), and hexagonal BN (h-BN). In most such systems that are termed van der Waals (vdW) heterostructures [15], the equilibrium interlayer distance is higher than or in the range of their lattice constant, and interlayer interactions are much weaker than intralayer interactions.

Another emerging class of 2D vertical heterostructures is that with quasi-bonding or covalent bonds where interlayer distances are considerably (1 Å to 2 Å) smaller than vdWHs. Initially, a metastable structure of bilayer graphene had been reported with an interlayer distance of 1.56 Å [16]. Recently, it is also shown that the decreasing interlayer distance in donor–acceptor heterostructures can significantly alter the band structure and give rise to novel phenomena that cannot be achieved in the case of vdW heterostructures [17]. The covalent interlayer bonding was also reported in the case of layered TMDs [18], bilayer borophene [19], borophene/graphene [20,21] and borophene/graphenylene bilayer [22]. Besides, non-vdW heterostructures are reported to be the most favorable structures of bilayer CdO [23] and MgO/ZnO heterostructures [24].

The reports above show a possible new path in designing novel heterostructures with outstanding physical properties and the necessity

* Corresponding author.
E-mail address: tanatar@fen.bilkent.edu.tr (B. Tanatar).

https://doi.org/10.1016/j.commatsci.2023.112712
Received 16 June 2023; Received in revised form 20 October 2023; Accepted 30 November 2023
Available online 8 December 2023

of further examinations. Although several works have shown the possibility of assembling heterostructures from MLs with different symmetry and lattice constants [25–29], the most straightforward structures are those formed by MLs with close lattice matching. Specifically, having a small number of atoms in the unit cell eases the computational study with high accuracy by employing advanced methods.

In this work, utilizing first principle calculations based on density functional theory (DFT), we investigated four possible heterostructures formed by CdO and SnC MLs. Previous works reported lattice constants of 3.59 Å and 3.55 Å for CdO and SnC, respectively [30,31]. The lattice mismatch between these graphenelike planar MLs is less than the lattice mismatch between the graphene and h-BN (1.8%) [32,33] making them promising for assembling heterostructures.

In its bulk phase, CdO has a rocksalt structure and is an n-type semiconductor [34]. It belongs to the family of metal oxides where optical transparency is incorporated with high carrier mobilities, which is essential in transparent circuits [35]. Due to high electrical conductivity in the energy range of visible light, CdO thin films are adequate for optoelectronic [36]. The room temperature direct band gap of CdO thin films is measured as 2.18 eV [37] and it is shown that upon donor doping, the band gap is controllable for full-spectrum photovoltaics [38,39]. The mechanical and dynamical stability of ML graphenelike CdO is demonstrated via DFT calculations [30,40,41]. Also, it is shown that CdO has the smallest band gap among the group II oxide MLs [30]. A recent theoretical study based on GW approximation and solving the Bethe–Salpeter equation (BSE) [42] has reported the electronic and optical band gaps of CdO as 2.40 eV and 1.27 eV, respectively [43]. Possessing an optical band gap close to the maximum solar spectrum flux (1.4 eV), ML CdO is a good candidate for application for photovoltaics. Furthermore, semiconductor-to-metallic transition by simultaneous Cd and O vacancy and magnetization upon B and C doping are reported in CdO ML [44]. Due to these fascinating properties, layered heterostructures based on ML CdO also attracted many researchers. The potential application of CdO/PtS_2, CdO/HfS_2 [45], CdO/CdS [46], CdO/MoS_2 [47], and CdO/g-C_3N_4 [48] in water splitting are demonstrated employing ab-initio methods.

ML SnC is a member of the IV-IV binary planar graphene-like structures and similar to other tin-based materials, it has received attention in recent years, and its application in various fields has been investigated. A GW study has predicted an indirect (K $\rightarrow$ Γ) band gap of 2.43 eV that is adjustable by applying strain [49]. Furthermore, the feasibility of controlling the band structure of ML SnC via halogenation is also pointed out [50,51]. Theoretical studies has shown that ML SnC is a promising anode material for lithium and sodium batteries. Moreover, it is established that by employing chemical functionalization, the electronic structure of a SnC monolayer can be adjusted, resulting in the transition from an initially indirect to a direct band gap, accomplished through comprehensive halogenation and Janus-functionalization. Currently, the application of SnC-based heterobilayers in optoelectronic [52], thermoelectric [53], gas sensors [54,55], water splitting [56,57], and hydrogen storage is demonstrated.

Previously, it was shown that the most favorable structure of the ZnO/GeC hetero-bilayer is formed by placing Zn(O) on top of the Ge(C) atom [58,59]. An essential property of this structure is the interlayer distance of 2.8 Å which is smaller than the common vdW heterostructures. As mentioned before, in such structures, the electronic properties change unpredictably and can give rise to distinguished physical properties. Therefore, it is intriguing to study the heterostructures formed by binary structure from II-VI and IV-IV. To our knowledge, CdO/SnC heterostructures still need to be considered in the literature. Therefore, employing DFT, we first investigated the mechanical properties of CdO/SnC heterostructures in four different stackings. A dynamically stable phase at zero temperature is predicted by placing Cd(O) atom on top of the Sn(C), and its electronic and optical properties are explored utilizing GW approximation and solving the BSE equation.

The rest of this paper is organized as follows. In the next section we outline the computational details of our numerical calculations. In Section 3, we report our results on the stability analysis, mechanical, electronic and optical properties of the considered heterostructures. Finally, we summarize our conclusions in Section 4.

2. Computational details

We performed *ab initio* calculation based on DFT [60] and utilizing projector-augmented wave potentials [61,62] and generalized gradient approximation of Perdew, Burke, and Ernzerhof [63–65]. Recommended GW potentials are used in all steps of the calculations. Besides, the nonlocal vdW-DF of Hamada (rev-vdW-DF2) is employed to account for dispersion interactions. It is shown that rev-vdW-DF2 can generate lattice parameters consistent with experimental results for a wide range of materials [66]. The structures are fully relaxed by employing the conjugate gradient method and using parameters that are selected according to previous reports and results of the conducted convergence tests. Accordingly, the kinetic energy cutoff for the plane-wave basis is set to 500 eV, and a Γ-centered 35 × 35 × 1 k-point mesh is used for sampling the Brillouin zone (BZ). The convergence tolerance for the total energy of the system is set to be less than 10^{-7} eV, and the Hellmann-Feynman forces are minimized to be less than 10^{-3} eV/Å. Fast convergence is achieved using the Gaussian smearing method combined with a small width of 0.01 eV. A vacuum of 30 Å is considered above the layers to minimize the interaction between the periodic images. Subsequently, 5 × 5 × 1 supercell and 15 × 15 × 1 Γ-centered k-point are employed for calculating the second-order force constant within the framework of density functional perturbation theory [67,68].

We performed a single shot of GW (G_0W_0) approximation to overcome the usual underestimation of the band gap by DFT. A Γ-centered 18 × 18 × 1 k-point mesh is used in our G_0W_0 calculation. The obtained quasiparticle (QP) energies and eigenfunctions G_0W_0 used for constructing BSE in Tamm–Dancoff approximation (TDA) [42,69]. Due to excessive memory requirements, 6 occupied and 6 unoccupied bands are considered for solving the BSE. Similar parameters are used for driving the scaling universality between the QP band gap and exciton binding energy of 2D materials [70], except that we considered 800 empty bands to ensure the accuracy of our results. Further details about the selecting parameters can be found in the previous work [24]. Here, we emphasize that converged results for the BSE eigenvalues are only guaranteed using a very dense k-point mesh [71], i.e., up to 300 × 300 × 1. Besides, a coarse k-point mesh can lead to a large overestimation of the frequency-dependent dielectric function and other quantities related to optical properties, which are one the main concerns of this paper. As it is shown in Ref. [72], for 2D materials such as WS_2 and MoS_2, a 15 × 15 × 1 k-point mesh is required for obtaining the converged values of the frequency-dependent dielectric function.

3. Results

3.1. Stability analysis and mechanical properties

The relaxed structures of the considered CdO/SnC hetero-bilayers are depicted in Fig. 1. In the structure named AA_I, the Sn atom is placed on top of the Cd atom, and the C atom is on top of the O atom. In the AA_{II} structure, the position of Sn and C atoms in AA_I are exchanged. The AB_I and AB_{II} structures can be obtained by moving the upper layer by a bond length and in the direction of the bond between the Cd and O atoms. It is important to clarify that our goal here is to create a stable structure with a smaller interlayer distance compared to typical vdW heterostructures. Achieving this involves stacking at least one atom from each monolayer. Within this context, there are two structures similar to AB_I and AB_{II} study. These structures can be obtained by swapping the positions of Cd and O atoms within the AB_I

Table 1
Obtained values of in-plane lattice constant a, interlayer distance h, binding energy E_{bind}, stiffness coefficients C_{11} and C_{12}, Young's Modulus (Y), and Poisson's ratio ν for the considered structures.

Configuration	a (Å)	h (Å)	E_{bind} (meV)	C_{11} (N m^{-1})	C_{12} (N m^{-1})	(Y (N m^{-1}))	ν
AA_I	3.61	3.78	−120.65	174.22	98.40	118.60	0.565
AA_{II}	3.71	2.40	−813.00	106.82	52.520	80.1	0.490
AB_I	3.66	2.56	−439.83	117.23	73.62	70.1	0.628
AB_{II}	3.61	3.80	−128.94	174.52	99.23	80.10	0.490

and AB_{II} structures. However, due to the higher electronegativity of oxygen, it is expected that AB_I and AB_{II} structures would likely result in smaller interlayer distances. We first relaxed SnC and CdO MLs using PBE+vdW functionals. The obtained lattice constants for CdO and SnC are 3.65 Å and 3.60 Å, respectively. This implies a lattice mismatch of 1.4% between the structures. To ensure the accuracy of geometry optimization, we performed a full relaxation in the primary unit cell and a 2 × 2 × 1 supercell of the considered structures and obtained identical results.

According to the obtained lattice parameters that are summarized in Table 1, AA_{II} has a lattice constant of 3.71 Å which is the largest value among the assessed configuration. This maximum value is larger than the lattice constant of CdO and SnC by 1.6% and 3%, respectively. The lattice constants of AA_I and AB_{II} are smaller than the lattice constant of AA_{II} by 0.1 Å, while for AB_I this difference is only 0.05 Å. The interlayer distances of the AA_{II} and AB_I are smaller than the AA_I and AB_{II} by more than 1 Å, which indicates stronger interlayer interaction in the AA_{II} and AB_I structures.

The dissimilarity in calculated interlayer distances can be further clarified by comparing the binding energies (E_{bind}) between the layers:

$$E_{bind} = E_{tot} - (E_{CdO} + E_{SnC}) \quad (1)$$

where E_{tot} is the total energy of the heterostructure, and E_{CdO} and E_{SnC} are the energy of each ML in the corresponding structure. AA_{II} possesses prominent binding energy compared to the other configurations and is the most favorable structure thermodynamically. Besides, the AB_I structure also has a binding energy of −439.83 meV, which is smaller than the AA_I and AB_{II} structures by more than three times.

Since all structures are thermodynamically stable, we also examined their mechanical stabilities by calculating the stiffness elastic constants C_{ij}, using the energy-strain method [73,74]. The calculated elastic constants are given in Table 1. The obtained values for C_{ij} show that all materials are mechanically stable according to stability conditions for the crystals with hexagonal lattice symmetry ($C_{11} > |C_{12}|, C_{11} > 0$) [75,76]. Apart from the mechanical stability, the calculated elastic constants show the mechanical softness of the considered systems. This aligns with previous studies that reported ML CdO [77] and group II-VI mono-chalcogenides [78] as soft 2D materials with promising piezoelectric properties.

To confirm the dynamical stability of the considered materials, we calculated their phonon frequencies. The obtained phonon dispersion curves are presented in Fig. 2 and Ref. [79] Fig S1. Except for the AA_{II} configuration, the rest of the structures possess imaginary phonon frequencies in the middle part of the BZ. Hence, only the AA_{II} structure is dynamically stable at zero temperature. Accordingly, in the rest of this paper, we focus on investigating the electronic and optical properties of AA_{II} structure.

3.2. Electronic properties

Our DFT calculation predicts an indirect band gap (K → Γ) of 0.08 eV (see Fig. 3). A critical issue in describing the electronic properties of the considered structure is the possible effect of the spin–orbit coupling (SOC) due to the presence of the heavy element Sn. Unfortunately, SOC is not compatible with vdW functionals [80,81]. Thus we first start by justifying the framework followed in the current study. In the most of

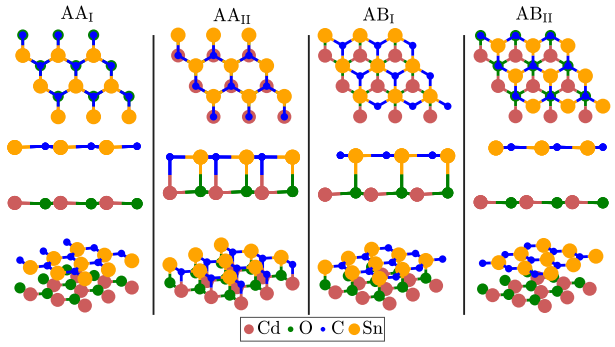

Fig. 1. Ball and stick representation of the relaxed structures of the considered CdO/SnC heterostructures.

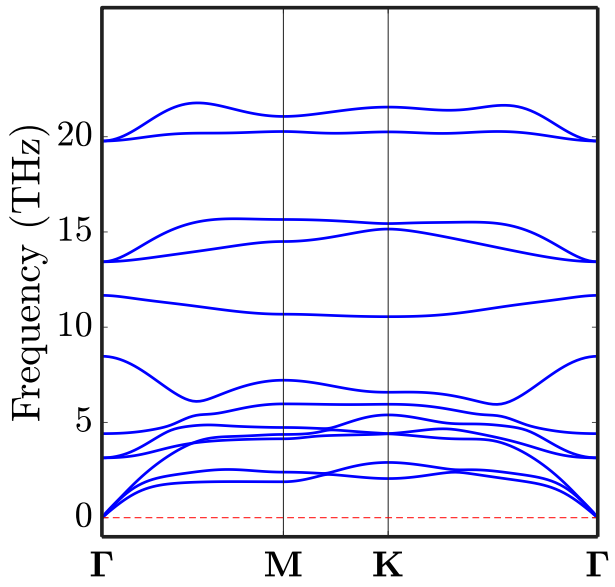

Fig. 2. Calculated phonon dispersion curves of the AA_{II} structure. Dashed red line shows zero frequency.

the previous studies on the electronic properties of the system consisted of the ML SnC, the effect of SOC is neglected. Also, it is shown that in the case of ML SnP and SnA, including SOC reduces the band gap by 0.05 eV for both materials [82]. In the specific case of ML SnC, a recent DFT study based on LDA functional has reported a reduction in the band gap from 1.246 eV to 1.12 eV by introducing the SOC effect, and the difference between the results of LDA and LDA+SOC is reported as 0.086 eV under 3% biaxial tensile strain [83]. As discussed in the previous section, the lattice constant of the AA_{II} layer is 3% larger than the relaxed ML SnC, and it might induce SOC effect in the range of the band gap. Here, following the approach of Wines et al. [81], we used the optimized geometry from the PBE+vdW and performed a noncolinear calculation to obtain the band structure including the SOC (see Ref. [79] Fig S6). Our results show a reduction of 10 meV in the band gap after including SOC, which is about 12.5% of the calculated

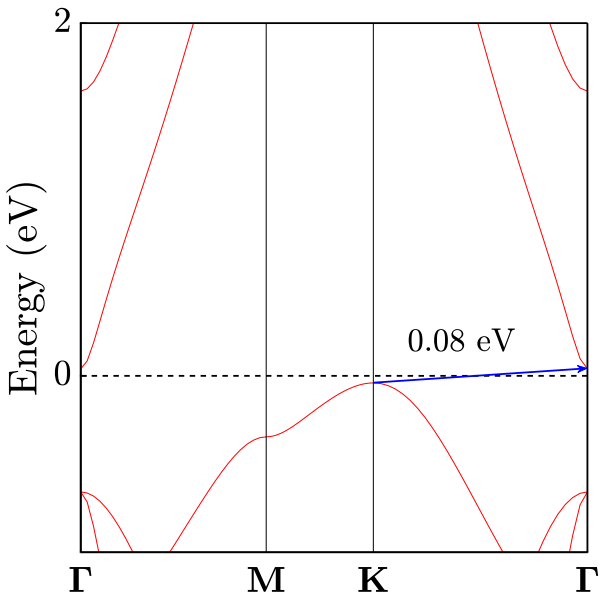

Fig. 3. DFT band structure of the AA_{II} structure. The Fermi energy is shifted to zero.

PBE+vdW band gap. However, it is well-known that PBE underestimates the band gap [84]. Later in this paper, we will apply the G_0W_0 approximation on top of the DFT results to obtain a more realistic band gap. We also calculated the band structure using the Heyd–Scuseria–Ernzerhof (HSE06) hybrid functional [85,86] (see Ref. [79] Fig S7). Our HSE result predicts an indirect band gap of 0.83 eV. More importantly, there is a close matching between the HSE+vdW and the PBE+vdW results for the two first conduction bands and two top valence bands. These results show the SOC can be neglected and PBE+vdW wave functions can be employed to reduce the computational cost of the GW and BSE steps.

After the above explanations, we continue with presenting the results of the PBE+vdW. Our results predicts a direct band gap of 0.75 eV at the Γ point for CdO, which is in close agreement with the previous reports [30,43]. For SnC, we obtained an indirect band gap of 0.90 eV, smaller than the previously reported LDA values [31,49]. However, it is in excellent agreement with the prediction of Ref. [87] where the vdW corrections are taken into account. In Fig. 4, we presented the contribution of each element in the band structure of the AA_{II} structure. The maximum of the valence band (VBM) is located at the K point, and the minimum of conduction band (CBM) is at the Γ point. The indirect nature of the band gap is similar to the ML SnC, and as can be seen from Fig. 4, the SnC layer has a dominant contribution to the valence band. Specifically, VBM is mainly formed by the orbitals of the carbon atom (see Ref. [79] Figs S2–S5 for orbital projected band structures). Near the Γ point, the contribution of the s orbitals of the SnC layer is more than the CdO layer, but it decreases toward the middle of the first BZ. The orbitals of SnC layer becomes dominant in the M-K path, where the p_z orbitals of the Sn atom form the first conduction band. The mixing between the orbitals of two layers at the Γ point differs from the common characteristic of vdWHs. In vdWHs, the VBM and CBM of the layers are usually well separated, showing one of the three types of conventional band alignments [88,89]. According to Fig. 4(c) due to dominant contribution of the SnC layer near the Γ point the band structure of the AA_{II} heterostructure resembles the type-I band alignment. DFT band gap of the AA_{II} structure is decreased by 89.40% and 90.10% compared with the DFT band gap of the ML CdO and SnC, respectively. This result, shows the substantial character of the interlayer interactions in the AA_{II} structure. To get further insight into interlayer interaction, we performed a Bader charge analysis [90–92]. According to the results summarized in Table 2, the layers are not

Table 2
The calculated Bader's charge associated with each atom in AA_{II} structure.

Cd	O	Sn	C
1.043	−1.169	1.475	−1.345

charged neutral as the CdO layer has received a negative charge of 0.126 e from the SnC layer. The charge transfer between the layers might be attributed to the higher electronegativity of the O atom.

We also calculated the electron localization function (ELF) [93,94] to further examine the interlayer interaction. In terms of the electron localization of uniform electron gas (D_e) and the kinetic energy densities of electron pairs (D_k) the ELF is given by:

$$\mathrm{ELF} = \left(1 + \left[\frac{D_k}{D_e}\right]^2\right)^{-1} \tag{2}$$

The ELF is a dimensionless quantity that varies between 0 and 1. The maximum and minimum values of the ELF correspond to completely non-localized and perfectly localized states, respectively. Besides, $0.2 < \mathrm{ELF} < 0.7$ indicates the metallic nature of the bond, and when ELF has a value around 0.75, close to the mid-distance between two atoms, the corresponding bond has a covalent nature [41,95–98]. In Fig. 5, we plotted an isosurface [99] of the ELF on the (1 1 0) plane containing all four atoms of the AA_{II} structure. One important feature deduced from the ELF function is the delocalization of the electrons around the Sn atom, and electrons are mostly localized around the O and C atoms. In the middle of the distance between the C and Sn atoms, the ELF has a value of around 0.6 which increases to 0.75 by moving toward the C atom and decreasing toward the Sn atom. This shows a mixed metallic-covalent bond between Sn and C atoms. In the half interlayer distance, there is a very narrow region with a small ELF value between the O and Sn atom. This gap in the ELF is slightly increased in the region between Cd and C atoms. This narrow gap in ELF distinguishes AA_{II} from the typical vdW structure, such as bilayer graphene, where ELF has a zero value in a considerable region between the layers [98].

Having illustrated the electronic properties at the DFT level, we focus on excited states and optical properties. First, we conducted a G_0W_0 calculation utilizing the DFT wavefunctions. The obtained G_0W_0 band structures are compared with the DFT result in Fig. 6. Although the DFT underestimates the band gap, the shape of the band structure does not change dramatically by including QP effects, as the G_0W_0 band structure can be fairly described by applying a scissor operator to the DFT results, specifically in the first valence and lowest conduction bands. Our GW calculation predicts a direct bandgap of 2.20 eV for CdO, which is in close agreement with the previous report [43]. The calculated indirect band gap of SnC is 1.91 eV, which is smaller than the previously reported value of 2.43 eV [49]. The reason is the fact that including the vdW correction changes the lattice parameter of the SnC. Besides, the results show that the AA_{II} structure possesses an indirect band gap of 1.10 eV. More importantly, at the Γ point, the AA_{II} structure also has a direct band gap of 1.65 eV, which is larger than the indirect band gap by 0.55 eV. The direct band gap of the AA_{II} structure is 0.57 eV smaller than the predicted band gap of CdO (2.22 eV). The slight difference between the direct and indirect band gaps is also a feature of the ML SnC [31], the main result of assembling these MLs in AA_{II} heterostructure is the considerable reduction in the fundamental band gap. The obtained indirect band gap is close to the band gap of silicon (1.17 eV), the widely used bulk semiconductor. However, the indirect band gap of silicon is 3.40 eV, which is unsuitable for visible light optoelectronic [100–102]. Hence, thick silicon layers are required to promote the phonon-assisted transitions. An essential property of 2D materials is their ability to absorb considerable amounts of light in a thickness of a few angstroms. For example, graphene can absorb light 2.3% of visible light [103,104], which is equivalent to the absorption

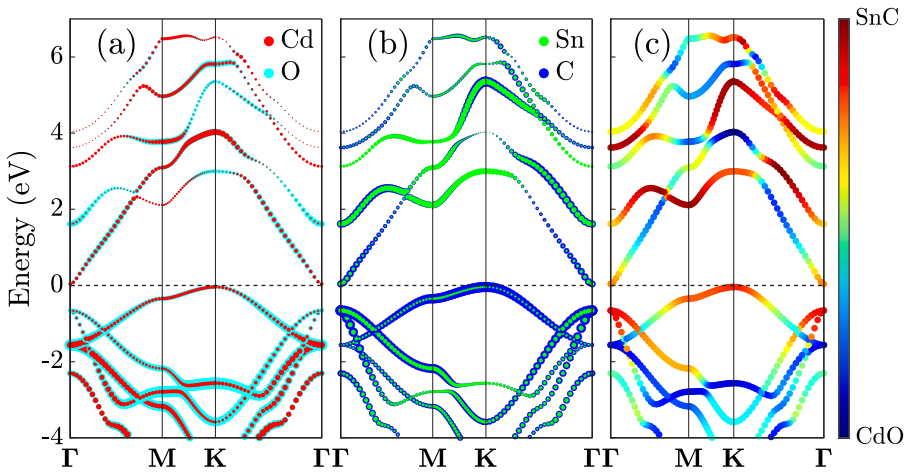

Fig. 4. (a) and (b) The contribution of the orbitals of each atom of CdO and SnC layers in the band structures of the AA_{II}, respectively. (c) The contribution of each layer in the band structure.

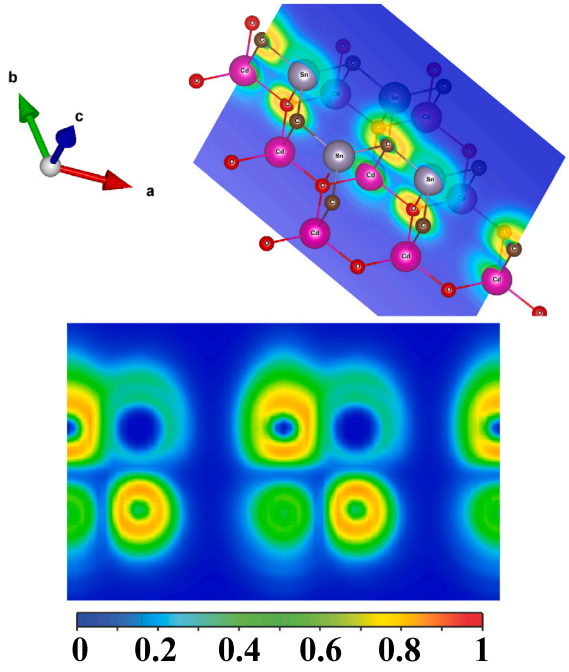

Fig. 5. Isosurface of the ELF on the (1 1 0) plane.

of 20 nm thick silicon. Furthermore, it is shown that some 2D materials with an indirect fundamental band gap possess optical properties that make them promising for optoelectronic [105–108]. As mentioned before, the G_0W_0 band structure can be obtained by applying a scissor operator to the DFT band structure that facilitates utilizing the band center approximation for obtaining the electron affinity [109,110]. Here, we obtained the valence and conduction band edge directly from the G_0W_0 calculation. According to the results that are depicted in Fig. 7(a), the work function of the AA_{II} is placed between the CdO and SnC monolayers, and the electron affinity is reduced in the AA_{II} structure. The reduction in the band gap of AA_{II} structure can be interpreted by the built-in potential differences in the heterostructure, as shown in AA_{II}(b). In Section 3.2, we identified AA_{II} heterostructure as type-I by considering the position of the valence and conduction bands of each layer. Considering the slight difference between the AA_{II} structure's direct and indirect band gaps, we investigated its optical properties in the next section.

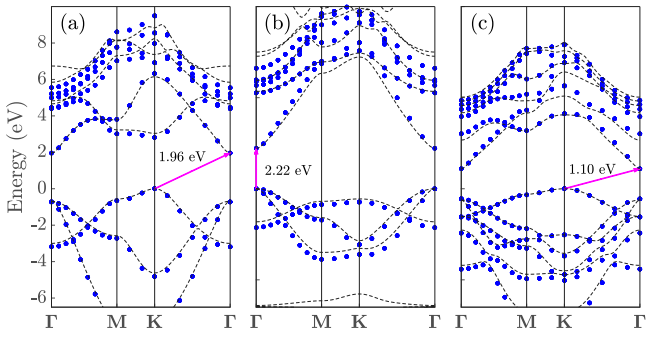

Fig. 6. Calculated G_0W_0 band structure of the SnC (a), CdO (b) and AA_{II} (c) (blue dots), the dashed line shows the DFT band structure. The conduction bands of the DFT are shifted by the difference between the band gaps of DFT and G_0W_0. The maximum of the valence bands are shifted to zero.

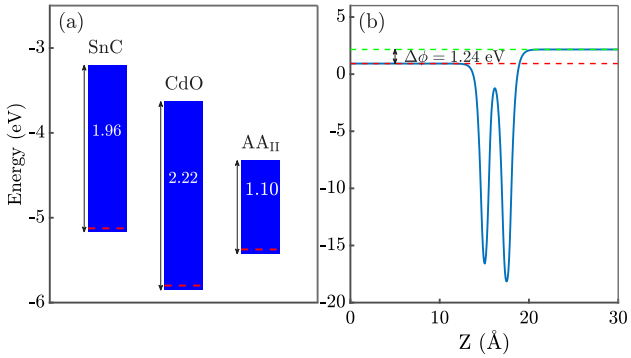

Fig. 7. (a) Band alignment of isolated SnC, CdO, and AA_{II}. The vacuum level is considered at zero, and dashed red lines show the position of the Fermi energy. (b) The planar average of the electrostatic potential along the z-direction of AA_{II} structure. $\Delta\phi$ shows the built-in voltage across the layer.

3.3. Optical properties

To examine the optical properties of AA_{II}, we solved BSE in TDA using the QP orbitals obtained in G_0W_0:

$$\left(E_{c\mathbf{k}} - E_{v\mathbf{k}}\right) A^{S}_{vc\mathbf{k}} + \sum_{v'c'\mathbf{k}'} K_{vc\mathbf{k},v'c'\mathbf{k}'}(\Omega^{S}) A^{S}_{v'c'\mathbf{k}'} = \Omega^{S} A^{S}_{vc\mathbf{k}} \quad (3)$$

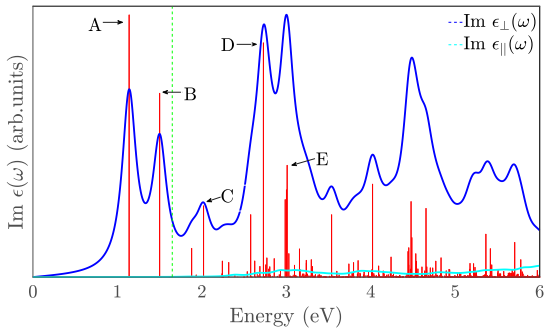

Fig. 8. Imaginary part of the dielectric function for perpendicular (Im$\epsilon_\perp(\omega)$) (blue) and parallel incident light (Im $\epsilon_\parallel(\omega)$) (cyan). The vertical red lines show the oscillator strengths. The dashed green line shows the position of the direct band gap obtained in G_0W_0. Table 3 lists the exciton energies and G_0W_0 of the peaks of the oscillator strengths that shown by letters.

Table 3
Calculated G_0W_0 direct band gap $E^d_{G_0W_0}$, exciton eigenvalue E_e, exciton binding energies E_b and the absorption A(ω) for the first five peaks of the imaginary part of the frequency dependent dielectric function of the AA_{II} structure (c.f. Fig. 8).

Peak name	$E^d_{G_0W_0}$ (eV)	E_e (eV)	E_b (eV)	A(ω) (%)
A	1.65	1.14	0.51	4.00
B	2.04	1.50	0.54	4.00
C	2.54	2.02	0.52	2.80
D	3.19	2.73	0.46	11.75
E	3.53	3.01	0.52	13.20

Here, $E_{c\mathbf{k}}$ ($E_{v\mathbf{k}}$) shows the energy of the electron (hole) obtained in G_0W_0 step, $A^S_{vc\mathbf{k}}$ denotes the exciton coupling coefficient, Ω^S is the exciton eigenvalue and $K_{vc\mathbf{k},v'c'\mathbf{k}'}$ is the electron–hole interaction kernel [111].

Fig. 8 shows our BSE results of the imaginary part of the frequency-dependent dielectric function of the AA_{II} structure for perpendicular Im $\epsilon_\perp(\omega)$ and parallel incident Im $\epsilon_\parallel(\omega)$ light. The oscillator strengths in Fig. 8 are normalized concerning the maximum of the Im $\epsilon_\perp(\omega)$ in the shown energy range. The oscillator strength is related to the coherent sum of the momentum matrix elements [112–115]. It can be used to quantify the intensity of transitions, as an exciton with zero oscillator strength is considered a dark exciton. Unlike the CdO, which possesses a single peak of Im $\epsilon_\perp(\omega)$ at its optical band gap [43], the Im $\epsilon_\perp(\omega)$ of AA_{II} shows five peaks before the ultraviolet (c.f. Table 3). The first peak of the AA_{II} that corresponds to the optical band gap is located at 1.14 eV and has the maximum oscillator strength. The peak at 2.73 eV has an oscillator strength close to the maximum observed value. The underlying electrons and holes coupling that affects the behavior of the dielectric function can be revealed by looking at the distribution of the electron–hole coupling coefficient in a specific exciton eigenvalue. The exciton eigenstate $|S\rangle$ is constructed based on the product of the electron–hole basis [116–118]:

$$|S\rangle = \sum_{vc\mathbf{k}} A^S_{vc\mathbf{k}} |vc\mathbf{k}\rangle \tag{4}$$

According to Eq. (4), the distribution of the exciton coupling coefficient in the reciprocal lattice can be used to determine the spatial extent of an exciton [12,119]. The excitons that are localized in the momentum space possess a large radius in the real space. Fig. 9 shows the fatband representation of the coupling coefficients of the four prominent oscillator strengths. The first bright exciton of AA_{II} has appeared in photon energy of 1.14 eV and is well localized around the Γ point, which means it is delocalized in real space. This exciton possesses a large binding energy of 0.51 eV (c.f. Table 3), which is a common characteristic of the excitons of 2D semiconductors. Similar to the first bright exciton, the excitons appearing at photon energies of 1.5 eV and 2.73 eV are localized around the Γ and M point, respectively.

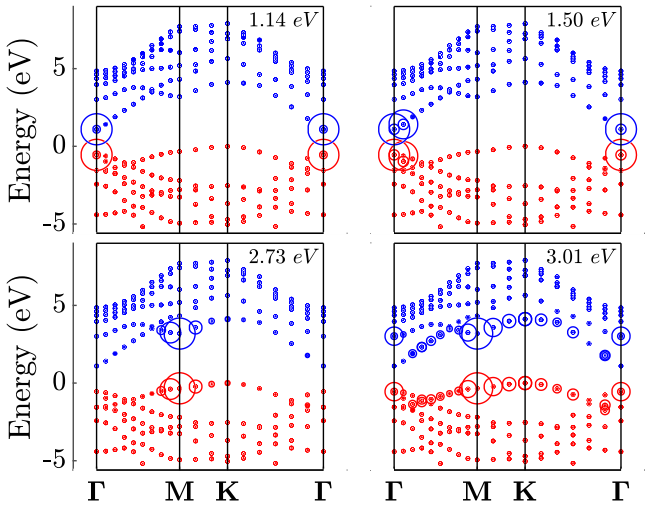

Fig. 9. The fatband representation of the absolute values of the coupling coefficients for the four prominent values of the oscillator strengths. The corresponding exciton eigenvalue is given in each subplot. Red and blue circles refer to holes and electrons, respectively.

On the other hand, the exciton that appears in the most prominent peak of the Im $\epsilon_\perp(\omega)$ has an eigenvalue of 3.01 eV and is not entirely localized at the M point. The coupling coefficients of this exciton are distributed in the BZ, and there is a local maximum at the Γ point. Thus one of the essential properties of AA_{II} structure is its multifunctionality due to possessing both real space localized and delocalized excitonic states.

Further insights into optical properties can be achieved by evaluating optical absorption. For 2D materials, the optical absorption A(ω) that shows the amount of light can be absorbed by the layer is defined based on 2D optical conductivity [120–122]:

$$\sigma_{2D}(\omega) = L\sigma_{3D}(\omega)$$
$$A(\omega) = \frac{\mathrm{Re}\ \frac{\sigma_{2D}(\omega)}{\epsilon_0 c}}{\left|1 + \frac{\sigma_{2D}(\omega)}{2\epsilon_0 c}\right|^2} \tag{5}$$

where L is the thickness of the slab, c is the speed of light, and ϵ_0 is the vacuum permittivity. Fig. 10 delivers the real part of the optical conductivity in units of universal conductivity of graphene [123] $\sigma_0 = \frac{e^2}{4\hbar} = 6.08 \times 10^{-5}\ \Omega^{-1}$. Similar to Im $\epsilon_\perp(\omega)$, the real part of the optical conductivity Re $\sigma(\omega)$ shows five peaks in energies less than ultraviolet light. However, two predominant peaks of the Re $\sigma(\omega)$ are located inside the visible light region. As explained before, the calculated values for frequency-dependent optical properties are very sensitive to the density of the employed k-point mesh, making the quantitative comparison difficult. However, the optical conductivity of the AA_{II} structures is comparable with the reported experimental values of TMDs, which are considered promising materials for optoelectronics [124–129]. Finally, we calculated the percentage of the light that can be absorbed by AA_{II} structure (see Ref. [79] Fig S8). The amounts of absorption at the first five peaks are given in Table 3. Before the visible light region, there are two peaks with 4%, and the absorption spectrum decreases after the second maximum at 1.51 eV. It receives a minimum value at 1.73 eV, where the layers can absorb 1.4% of the light, then increases until a local maximum in the red light region. Enhanced absorption is achieved for photon energies larger than red light, where there are two peaks with 11.75% and 13.2% absorption in the spectrum, and as it is explained before, the first is related to a spatially extended exciton, while the second peak corresponds to a localized exciton. These results show that AA_{II} structure can absorb light in a wide range of photon energies and is promising for optoelectronic.

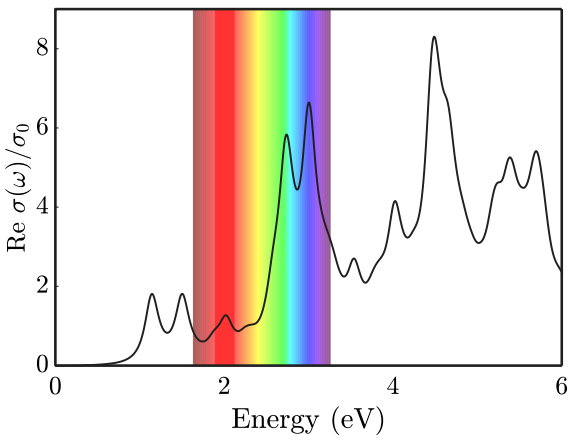

Fig. 10. Real part of the optical conductivity of AA_{II} structure, $\sigma_0 = \frac{e^2}{4\hbar}$.

4. Conclusion

We studied the mechanical and dynamic stabilities of CdO and SnC hetero-bilayers in four different stacking. Despite the mechanical stabilities of the considered structures, the phonon dispersion curves show that only the AA_{II} structure formed by placing the Sn(C) on top of the O(Cd) atom is dynamically stable at zero temperature. A notable characteristic of the AA_{II} structure is its larger lattice constant than its monolayer counterparts, as the lattice constant of AA_{II} is 3% larger than the SnC monolayer. It shows the possibility of assembling stable vertical heterostructures without a very close lattice matching, which is usually required for assembling vdWHs. Besides, AA_{II} possesses a smaller distance than the typical vdWHs and shows distinguishing electronic and optical properties. It has a narrower band gap than the CdO and SnC monolayers. Due to the charge transfer between the layers, contrary to vdWHs, there is a narrow region of electron delocalization in the ELF function. Unlike the ML CdO that has a single absorption peak before the visible light, the optical absorption of the AA_{II} possesses five peaks before the ultraviolet light. Analyzing the electron–hole coupling coefficients of the absorption peaks revealed the presence of the momentum-space localized excitons and a delocalized exciton, which shows the multifunctionality of the AA_{II} structures. Our results provide an example of remarkable electronic and optical properties that can be achieved by hetero-bilayers with strong interlayer interaction.

CRediT authorship contribution statement

Mahsa Seyedmohammadzadeh: Investigation, Validation, Writing, Editing. **Arash Mobaraki:** Investigation, Validation, Writing, Editing. **B. Tanatar:** Project administration, Funding acquision, Supervision, Writing, Editing. **Oğuz Gülseren:** Supervision, Writing, Editing.

Declaration of competing interest

The authors declare the following financial interests/personal relationships which may be considered as potential competing interests: Bilal Tanatar reports financial support was provided by Scientific and Technological Research Council of Turkey. Bilal Tanatar reports financial support was provided by Turkish Academy of Sciences.

Data availability

Data will be made available on request.

Acknowledgments

This work is supported by The Scientific and Technological Research Council of Turkey (TUBITAK) under Grant No. 119N086 and Turkish Academy of Sciences (TUBA). Computational resources were provided by the High Performance and Grid Computing Center (TRGrid e-Infrastructure) of TUBITAK ULAKBIM, Turkish Academic Network and Information Center. We thank Cem Sevik for useful comments.

Appendix A. Supplementary data

Supplementary material related to this article can be found online at https://doi.org/10.1016/j.commatsci.2023.112712.

References

[1] K.S. Novoselov, A.K. Geim, S.V. Morozov, D. Jiang, Y. Zhang, S.V. Dubonos, I.V. Grigorieva, A.A. Firsov, Science 306 (5696) (2004) 666–669.
[2] V. Meunier, A.G. Souza Filho, E.B. Barros, M.S. Dresselhaus, Rev. Modern Phys. 88 (2016) 025005.
[3] A.H. Castro Neto, F. Guinea, N.M.R. Peres, K.S. Novoselov, A.K. Geim, Rev. Modern Phys. 81 (2009) 109–162.
[4] K. Khan, A.K. Tareen, M. Aslam, R. Wang, Y. Zhang, A. Mahmood, Z. Ouyang, H. Zhang, Z. Guo, J. Mater. Chem. C 8 (2020) 387–440.
[5] M. Zeng, Y. Xiao, J. Liu, K. Yang, L. Fu, Chem. Rev. 118 (13) (2018) 6236–6296.
[6] X. Li, Z. Huang, C.E. Shuck, G. Liang, Y. Gogotsi, C. Zhi, Nat. Rev. Chem. 6 (6) (2022) 389–404.
[7] S. Bai, M. Yang, J. Jiang, X. He, J. Zou, Z. Xiong, G. Liao, S. Liu, Npj 2D Mater. Appl. 5 (1) (2021) 78.
[8] C. Cui, F. Xue, W.-J. Hu, L.-J. Li, Npj 2D Mater. Appl. 2 (1) (2018) 18.
[9] B. Zhang, J. Zhou, Z. Sun, J. Mater. Chem. A 10 (2022) 15865–15880.
[10] A. Chaves, J.G. Azadani, H. Alsalman, D.R. da Costa, R. Frisenda, A.J. Chaves, S.H. Song, Y.D. Kim, D. He, J. Zhou, A. Castellanos-Gomez, F.M. Peeters, Z. Liu, C.L. Hinkle, S.-H. Oh, P.D. Ye, S.J. Koester, Y.H. Lee, P. Avouris, X. Wang, T. Low, Npj 2D Mater. Appl. 4 (1) (2020) 29.
[11] Z. Peng, X. Chen, Y. Fan, D.J. Srolovitz, D. Lei, Light: Sci. Appl. 9 (1) (2020) 190.
[12] P.H. López, S. Heeg, C. Schattauer, S. Kovalchuk, A. Kumar, D.J. Bock, J.N. Kirchhof, B. Höfer, K. Greben, D. Yagodkin, L. Linhart, F. Libisch, K.I. Bolotin, Nature Commun. 13 (1) (2022) 7691.
[13] A. Ramasubramaniam, D. Naveh, E. Towe, Phys. Rev. B 84 (2011) 205325.
[14] D. Wang, X.-B. Li, H.-B. Sun, Nano Lett. 21 (14) (2021) 6298–6303.
[15] A.K. Geim, I.V. Grigorieva, Nature 499 (7459) (2013) 419–425.
[16] P.L. de Andres, R. Ramírez, J.A. Vergés, Phys. Rev. B 77 (2008) 045403.
[17] A.H. Woomer, D.L. Druffel, J.D. Sundberg, J.T. Pawlik, S.C. Warren, J. Am. Chem. Soc. 141 (26) (2019) 10300–10308.
[18] X. Zhao, P. Song, C. Wang, A.C. Riis-Jensen, W. Fu, Y. Deng, D. Wan, L. Kang, S. Ning, J. Dan, T. Venkatesan, Z. Liu, W. Zhou, K.S. Thygesen, X. Luo, S.J. Pennycook, K.P. Loh, Nature 581 (7807) (2020) 171–177.
[19] X. Liu, Q. Li, Q. Ruan, M.S. Rahn, B.I. Yakobson, M.C. Hersam, Nature Mater. 21 (1) (2022) 35–40.
[20] A. Kochaev, R. Meftakhutdinov, R. Sibatov, K. Katin, M. Maslov, V. Efimov, Appl. Surf. Sci. 562 (2021) 150150.
[21] A. Kochaev, K. Katin, M. Maslov, R. Meftakhutdinov, J. Phys. Chem. Lett. 11 (14) (2020) 5668–5673.
[22] A. Kochaev, K. Katin, M. Maslov, S. Singh, Phys. Rev. B 105 (2022) 235444.
[23] D. Hoat, M. Naseri, T.V. Vu, J. Rivas-Silva, N.N. Hieu, G.H. Cocoletzi, Superlattices Microstruct. 145 (2020) 106644.
[24] M. Seyedmohammadzadeh, C. Sevik, O. Gülseren, Phys. Rev. Mater. 6 (2022) 104004.
[25] X. Liu, M.C. Hersam, Sci. Adv. 5 (10) (2019) eaax6444.
[26] G.-C. Guo, D. Wang, X.-L. Wei, Q. Zhang, H. Liu, W.-M. Lau, L.-M. Liu, J. Phys. Chem. Lett. 6 (24) (2015) 5002–5008.
[27] Q. Li, J. Yang, L. Zhang, J. Phys. Chem. C 122 (32) (2018) 18294–18303.
[28] P. Vishnoi, K. Pramoda, U. Gupta, M. Chhetri, R.G. Balakrishna, C.N.R. Rao, ACS Appl. Mater. Interfaces 11 (31) (2019) 27780–27787.
[29] S. Qin, H. Jiang, Q. Du, Z. Nie, X. Wang, W. Wang, X. Wang, Y. Xu, Y. Shi, R. Zhang, F. Wang, Carbon 146 (2019) 486–490.
[30] H. Zheng, X.-B. Li, N.-K. Chen, S.-Y. Xie, W.Q. Tian, Y. Chen, H. Xia, S.B. Zhang, H.-B. Sun, Phys. Rev. B 92 (2015) 115307.
[31] H. Şahin, S. Cahangirov, M. Topsakal, E. Bekaroglu, E. Akturk, R.T. Senger, S. Ciraci, Phys. Rev. B 80 (2009) 155453.
[32] G. Giovannetti, P.A. Khomyakov, G. Brocks, P.J. Kelly, J. van den Brink, Phys. Rev. B 76 (2007) 073103.
[33] L. Liu, Y.P. Feng, Z.X. Shen, Phys. Rev. B 68 (2003) 104102.
[34] M. Burbano, D.O. Scanlon, G.W. Watson, J. Am. Chem. Soc. 133 (38) (2011) 15065–15072.

[35] H. Hosono, Thin Solid Films 515 (15) (2007) 6000–6014.
[36] S.A. Khan, S. Azam, F.A. Shah, B. Amin, Opt. Mater. 47 (2015) 372–378.
[37] S.K. Vasheghani Farahani, V. Muñoz-Sanjosé, J. Zúñiga Pérez, C.F. McConville, T.D. Veal, Appl. Phys. Lett. 102 (2) (2013) 022102.
[38] C.P. Liu, Y. Foo, M. Kamruzzaman, C.Y. Ho, J.A. Zapien, W. Zhu, Y.J. Li, W. Walukiewicz, K.M. Yu, Phys. Rev. A 6 (2016) 064018.
[39] A. Shameem, P. Devendran, V. Siva, M. Raja, S.A. Bahadur, A. Manikandan, J. Inorg. Organomet. Polym. Mater. 27 (3) (2017) 692–699.
[40] H.L. Zhuang, R.G. Hennig, Appl. Phys. Lett. 103 (21) (2013) 212102.
[41] B. Luo, Y. Yao, E. Tian, H. Song, X. Wang, G. Li, K. Xi, B. Li, H. Song, L. Li, Proc. Natl. Acad. Sci. 116 (35) (2019) 17213–17218.
[42] L. Hedin, Phys. Rev. 139 (1965) A796–A823.
[43] Y.-m. Ding, X. Nie, Y. Li, Phys. Rev. Mater. 5 (2021) 074005.
[44] R. Chaurasiya, A. Dixit, J. Magn. Magn. Mater. 469 (2019) 279–288.
[45] Q. Zhang, K. Ren, R. Zheng, Z. Huang, Z. An, Z. Cui, Front. Chem. 10 (2022).
[46] G. Wang, L. Gong, Z. Li, B. Wang, W. Zhang, B. Yuan, T. Zhou, X. Long, A. Kuang, Phys. Chem. Chem. Phys. 22 (2020) 9587–9592.
[47] Z.-H. Yan, Y. Zhang, H. Qiao, L. Duan, L. Ni, Thin Solid Films 764 (2023) 139626.
[48] G. Wang, Y. Zhi, L. Xia, J. Chang, B. Yuan, X. Guo, Y. Li, S. Xiao, H. Yuan, Phys. Status Solidi (a) 217 (8) (2020) 1900859.
[49] T.-Y. Lü, X.-X. Liao, H.-Q. Wang, J.-C. Zheng, J. Mater. Chem. 22 (2012) 10062–10068.
[50] S. Majidi, S.M. Elahi, A. Esmailian, F. Kanjouri, Silicon 10 (3) (2018) 869–877.
[51] D.M. Hoat, M. Naseri, R. Ponce-Péreze, N.N. Hieu, J.F. Rivas-Silva, T.V. Vu, H.D. Tong, G.H. Cocoletzi, Mater. Res. Express 7 (1) (2019) 015013.
[52] R. Sheng, X. Deng, Z. Zhang, Z. Fan, Phys. Lett. A 384 (7) (2020) 126150.
[53] S. Insad, F. Ramadan, L. Drissi, N. Hassanain, E. Saidi, J. Phys. Chem. Solids 155 (2021) 110105.
[54] A.L. Marcos-Viquez, Á. Miranda, M. Cruz-Irisson, L.A. Pérez, Mater. Lett. 294 (2021) 129751.
[55] A.L. Marcos-Viquez, Á. Miranda, M. Cruz-Irisson, L.A. Pérez, Mater. Lett. 298 (2021) 130030.
[56] Z.-N. Dai, Y. Cao, W.J. Yin, W. Sheng, Y. Xu, J. Phys. D: Appl. Phys. 55 (31) (2022) 315503.
[57] A.L. Marcos-Viquez, A. Miranda, M. Cruz-Irisson, L.A. Pérez, Int. J. Hydrogen Energy 47 (97) (2022) 41329–41335.
[58] X. Gao, Y. Shen, Y. Ma, S. Wu, Z. Zhou, J. Mater. Chem. C 7 (2019) 4791–4799.
[59] G. Wang, L. Zhang, Y. Li, W. Zhao, A. Kuang, Y. Li, L. Xia, Y. Li, S. Xiao, J. Phys. D: Appl. Phys. 53 (1) (2019) 015104.
[60] W. Kohn, L.J. Sham, Phys. Rev. 140 (1965) A1133–A1138.
[61] P.E. Blöchl, Phys. Rev. B 50 (1994) 17953–17979.
[62] G. Kresse, D. Joubert, Phys. Rev. B 59 (1999) 1758–1775.
[63] J.P. Perdew, K. Burke, M. Ernzerhof, Phys. Rev. Lett. 77 (1996) 3865–3868.
[64] G. Kresse, J. Hafner, Phys. Rev. B 47 (1993) 558–561.
[65] G. Kresse, J. Furthmüller, Comput. Mater. Sci. 6 (1) (1996) 15–50.
[66] I. Hamada, Phys. Rev. B 89 (2014) 121103.
[67] S. Baroni, S. de Gironcoli, A. Dal Corso, P. Giannozzi, Rev. Modern Phys. 73 (2001) 515–562.
[68] A. Togo, I. Tanaka, Scr. Mater. 108 (2015) 1–5.
[69] S.M. Dancoff, Phys. Rev. 78 (1950) 382–385.
[70] Z. Jiang, Z. Liu, Y. Li, W. Duan, Phys. Rev. Lett. 118 (2017) 266401.
[71] D.Y. Qiu, F.H. da Jornada, S.G. Louie, Phys. Rev. B 93 (2016) 235435.
[72] H. Shi, H. Pan, Y.-W. Zhang, B.I. Yakobson, Phys. Rev. B 87 (2013) 155304.
[73] Y. Le Page, P. Saxe, Phys. Rev. B 63 (2001) 174103.
[74] V. Wang, N. Xu, J.-C. Liu, G. Tang, W.-T. Geng, Comput. Phys. Comm. 267 (2021) 108033.
[75] M. Madziarz, 2D Mater. 6 (4) (2019) 048001.
[76] S. Haastrup, M. Strange, M. Pandey, T. Deilmann, P.S. Schmidt, N.F. Hinsche, M.N. Gjerding, D. Torelli, P.M. Larsen, A.C. Riis-Jensen, J. Gath, K.W. Jacobsen, J.J. Mortensen, T. Olsen, K.S. Thygesen, 2D Mater. 5 (4) (2018) 042002.
[77] M.N. Blonsky, H.L. Zhuang, A.K. Singh, R.G. Hennig, ACS Nano 9 (10) (2015) 9885–9891.
[78] C. Sevik, D. Çakır, O. Gülseren, F.M. Peeters, J. Phys. Chem. C 120 (26) (2016) 13948–13953.
[79] Supplemental materials for An ab initio study of vertical heterostructures formed by CdO and SnC monolayers.
[80] J. Klimeš, D.R. Bowler, A. Michaelides, J. Phys.: Condens. Matter 22 (2) (2009) 022201.
[81] D. Wines, K. Choudhary, F. Tavazza, J. Phys. Chem. C 127 (2) (2023) 1176–1188.
[82] L. Rao, G. Tang, J. Hong, Phys. Rev. Mater. 7 (2023) 014010.
[83] M.R. Islam, Z. Wang, S. Qu, K. Liu, Z. Wang, J. Comput. Electron. 20 (1) (2021) 151–160.
[84] J.P. Perdew, Int. J. Quantum Chem. 28 (S19) (1985) 497–523.
[85] J. Heyd, J.E. Peralta, G.E. Scuseria, R.L. Martin, J. Chem. Phys. 123 (17) (2005) 174101.
[86] T.M. Henderson, J. Paier, G.E. Scuseria, Phys. Status Solidi (b) 248 (4) (2011) 767–774.
[87] H. Chen, J. Han, X. Deng, Z. Fan, L. Sun, Z. Zhang, Appl. Surf. Sci. 598 (2022) 153756.
[88] V.O. Özçelik, J.G. Azadani, C. Yang, S.J. Koester, T. Low, Phys. Rev. B 94 (2016) 035125.
[89] Y. Si, H.-Y. Wu, J.-C. Lian, W.-Q. Huang, W.-Y. Hu, G.-F. Huang, Phys. Chem. Chem. Phys. 22 (2020) 3037–3047.
[90] E. Sanville, S.D. Kenny, R. Smith, G. Henkelman, J. Comput. Chem. 28 (5) (2007) 899–908.
[91] G. Henkelman, A. Arnaldsson, H. Jónsson, Comput. Mater. Sci. 36 (3) (2006) 354–360.
[92] W. Tang, E. Sanville, G. Henkelman, J. Phys.: Condens. Matter 21 (8) (2009) 084204.
[93] A.D. Becke, K.E. Edgecombe, J. Chem. Phys. 92 (9) (1990) 5397–5403.
[94] B. Silvi, A. Savin, Nature 371 (6499) (1994) 683–686.
[95] Q.-Y. Chen, F.-J. Huang, J.-Q. Ruan, T. Ma, K. Xiong, Y. He, Phys. Rev. Mater. 6 (2022) 104005.
[96] R.J. Clements, J.C. Womack, C.-K. Skylaris, Electron. Struct. 2 (2) (2020) 027001.
[97] M. Abboud, D.H. Ozbey, M.E. Kilic, E. Durgun, J. Phys. D: Appl. Phys. 55 (18) (2022) 185302.
[98] K. Koumpouras, J.A. Larsson, J. Phys.: Condens. Matter 32 (31) (2020) 315502.
[99] K. Momma, F. Izumi, J. Appl. Crystallogr. 44 (6) (2011) 1272–1276.
[100] M.S. Hybertsen, S.G. Louie, Phys. Rev. Lett. 55 (1985) 1418–1421.
[101] P. Lautenschlager, M. Garriga, L. Vina, M. Cardona, Phys. Rev. B 36 (1987) 4821–4830.
[102] W. Zhang, C. Chai, Q. Fan, Y. Song, Y. Yang, Results Phys. 18 (2020) 103271.
[103] G. Pirruccio, L. Martín Moreno, G. Lozano, J. Gómez Rivas, ACS Nano 7 (6) (2013) 4810–4817.
[104] A.B. Kuzmenko, E. van Heumen, F. Carbone, D. van der Marel, Phys. Rev. Lett. 100 (2008) 117401.
[105] Y. Wu, Z. Tang, W. Xia, W. Gao, F. Jia, Y. Zhang, W. Zhu, W. Zhang, P. Zhang, Npj Comput. Mater. 8 (1) (2022) 129.
[106] Y. Jing, Y. Ma, Y. Li, T. Heine, Nano Lett. 17 (3) (2017) 1833–1838.
[107] M. Grzeszczyk, K.S. Novoselov, M. Koperski, Proc. Natl. Acad. Sci. 119 (41) (2022) e2207074119.
[108] M.E. Kilic, S.E. Rad, S. Ipek, S. Jahangirov, Phys. Rev. Mater. 6 (2022) 064007.
[109] Y. Liang, S. Huang, R. Soklaski, L. Yang, Appl. Phys. Lett. 103 (4) (2013) 042106, https://pubs.aip.org/aip/apl/article-pdf/doi/10.1063/1.4816517/14289461/042106_1_online.pdf.
[110] A. Slassi, S.M. Gali, A. Pershin, A. Gali, J. Cornil, D. Beljonne, J. Phys. Chem. Lett. 11 (11) (2020) 4503–4510, https://doi.org/10.1021/acs.jpclett.0c00780, PMID: 32419458.
[111] X. Leng, F. Jin, M. Wei, Y. Ma, WIREs Comput. Mol. Sci. 6 (5) (2016) 532–550.
[112] S. Sagmeister, C. Ambrosch-Draxl, Phys. Chem. Chem. Phys. 11 (2009) 4451–4457.
[113] F. Fuchs, C. Rödl, A. Schleife, F. Bechstedt, Phys. Rev. B 78 (2008) 085103.
[114] P. Liu, B. Kim, X.-Q. Chen, D.D. Sarma, G. Kresse, C. Franchini, Phys. Rev. Mater. 2 (2018) 075003.
[115] E. Ridolfi, C.H. Lewenkopf, V.M. Pereira, Phys. Rev. B 97 (2018) 205409.
[116] M. Bokdam, T. Sander, A. Stroppa, S. Picozzi, D.D. Sarma, C. Franchini, G. Kresse, Sci. Rep. 6 (1) (2016) 28618.
[117] T. Sander, E. Maggio, G. Kresse, Phys. Rev. B 92 (2015) 045209.
[118] M. Rohlfing, S.G. Louie, Phys. Rev. B 62 (2000) 4927–4944.
[119] R. Laskowski, N.E. Christensen, P. Blaha, B. Palanivel, Phys. Rev. B 79 (2009) 165209.
[120] L. Matthes, O. Pulci, F. Bechstedt, New J. Phys. 16 (10) (2014) 105007.
[121] L. Matthes, O. Pulci, F. Bechstedt, Phys. Rev. B 94 (2016) 205408.
[122] Z. Torbatian, R. Asgari, Phys. Rev. B 98 (2018) 205407.
[123] K.F. Mak, M.Y. Sfeir, Y. Wu, C.H. Lui, J.A. Misewich, T.F. Heinz, Phys. Rev. Lett. 101 (2008) 196405.
[124] Y. Li, A. Chernikov, X. Zhang, A. Rigosi, H.M. Hill, A.M. van der Zande, D.A. Chenet, E.-M. Shih, J. Hone, T.F. Heinz, Phys. Rev. B 90 (2014) 205422.
[125] P.K. Nayak, C.-H. Yeh, Y.-C. Chen, P.-W. Chiu, ACS Appl. Mater. Interfaces 6 (18) (2014) 16020–16026.
[126] B. Song, H. Gu, M. Fang, Y.-T. Ho, X. Chen, H. Jiang, S. Liu, J. Phys. Chem. Lett. 10 (20) (2019) 6246–6252.
[127] G.Y. Jia, Y. Liu, J.Y. Gong, D.Y. Lei, D.L. Wang, Z.X. Huang, J. Mater. Chem. C 4 (2016) 8822–8828.
[128] M. Fang, H. Gu, B. Song, Z. Guo, S. Liu, Adv. Photonics Res. 3 (4) (2022) 2100299.
[129] H. Wang, C. Zhang, F. Rana, Nano Lett. 15 (12) (2015) 8204–8210.